INPOP06. A new numerical planetary ephemeris

A. Fienga[1,2], H. Manche[1], J. Laskar[1], and M. Gastineau[1]

[1] Astronomie et Systèmes Dynamiques, IMCCE-CNRS UMR8028, 77 Av. Denfert-Rochereau, 75014 Paris, France
[2] Observatoire de Besançon

October 20, 2006

Abstract. INPOP06 is the new numerical planetary ephemeris developed at the IMCCE-Observatoire de Paris. INPOP (Intégrateur Numérique Planétaire de l'Observatoire de Paris) is a numerical integration of the motion of the nine planets and the Moon fitted to the most accurate available planetary observations. It also integrates the motion of 300 perturbing main belt asteroids, the rotation of the Earth and the Moon libration. We used more than 45000 observations including the last tracking data of the Mars Global Surveyor (MGS) and Mars Odyssey (MO) missions. The accuracy obtained with INPOP06 is comparable to the last versions of the JPL DE solutions (DE414, Konopliv et al. 2006) and of the EPM solutions (EPM04, Pitjeva 2005). First comparisons on tracking data of the new European space mission, Mars Express (MEX), are also included.

Key words. celestial mechanics - ephemeris

1. Introduction

The launch by NASA of the first interplanetary missions implied a considerable and continuous effort to develop and improve planetary ephemerides. The Jet Propulsion Laboratory (JPL) was entrusted with this task and produced over the years many solutions combining the best theories and the most recent observational techniques, such as range measurements or VLBI tracking. The major changes in observational accuracy (Lunar Laser Ranging, range and VLBI spacecraft tracking) permitted by modern technology, and in response to more demanding needs, have led to comparable improvements in the accuracy of the planetary and lunar ephemerides. Based on some first versions of numerical integration of planetary motions (see for instance Cohen et al., 1967), the DE102 JPL ephemerides (Newhall et al., 1983) were the first accurate numerical ephemerides fitted to observations developed by JPL. On the same scheme, came out successively DE200, DE403 (Standish et al., 1995) and DE405 (Standish, 1998). All these ephemerides are numerically integrated with a variable step-size, variable-order, Adams method. Their dynamical model includes point-mass interactions between the nine planets, the Sun and asteroids, relativistic PPN effects (Moyer, 2000), figure effects, Earth tides and lunar librations (Newhall et al., 1983). Since DE102, some improvements were added to the DE solutions, and new solutions such as DE409 (Standish, 2004), DE410 (Standish, 2005) and DE414 (Konopliv et al., 2006) were constructed and fitted on more and more dense sets of space missions tracking data. Numerical solutions have also being developed at the Institute of Applied Astronomy of Saint-Petersburg. They are based on a dynamical model very similar to the JPL one. These solutions, EPM, are also fitted to space tracking data and have an accuracy comparable to the JPL ephemerides (see for instance Pitjeva, 2005).

For many years, the accurate planetary ephemerides built at the JPL have been the only source of numerical ephemerides readily available. Besides the two numerical solutions presented above, the IMCCE developed since the early 80's, some analytical solutions for the planetary motion. However, despite their usefulness in some analytical computations, these solutions have a limited accuracy over short periods of time. For Mars, the intrinsic accuracy of the analytical solution (series limitation accuracy) is about 100 meters over 30 years (Fienga and Simon, 2005). Over the same interval of time the mean accuracy of Viking, Pathfinder and MGS tracking data is about 10 meters. It appears thus clearly that these analytical solutions are not accurate enough to be used in the data analysis of space missions.
Consequently, a new aspect of the IMCCE planetary ephemerides evolution arose with the development of a numerical solution of the planet motion called INPOP (Intégration Numérique Planétaire de l'Observatoire de Paris). This project sprang up in 2003 from the needs of accuracy of short term ephemeris for the analysis of Earth based and space mission observational data but also from the necessity of improvements in the dynamical model for the long term astronomical solutions used for the

Send offprint requests to: A. Fienga, fienga@imcce.fr

paleoclimate studies of the Earth and Mars over several millions of years. Indeed, because of the chaotic behavior of the orbital solutions of the Solar System (Laskar, 1989, 1990), extending the astronomical solutions from 40 Myr (Laskar et al. 2004a,b) to 60 Myr, corresponds to a gain of two orders of magnitude on the precision of the model and parameters. For these reasons, IMCCE decided to develop a new numerical planetary ephemeris adjusted to space mission tracking observations. INPOP has to be accurate on very short periods of time, but must also be extended over very long time intervals of several millions years.

In this paper, we present the latest version of our short term ephemeris INPOP, INPOP06. We describe the dynamical model used for the integration of the planets and Moon motions and the Earth and Moon rotations. We compare our model with the DE405 solution (Standish, 1998). This first step is important for the validation of our study, as we demonstrate that we can recover the DE405 solution in a very precise way. In a second part, we describe the fit made to observations. We present the observation processing and the residuals obtained with INPOP as well as with other available solutions such as DE405, DE410 and DE414. Two INPOP versions are obtained: the first one, INPOP05, mimicking DE405 in the dynamical model and data fit, and the other one, INPOP06, developed independently and fitted on available data till early 2006. New determinations of physical parameters such as asteroid masses and Sun oblateness are presented and compared to other values found in the literature.
Comparisons to Mars Express (MEX) tracking observations which were not used in any fit of any planetary solutions DE or INPOP are done. Such comparisons estimate the extrapolation capabilities of each planetary ephemeris.

2. The INPOP dynamical model

2.1. General features

INPOP is a numerical integration of the equations of motion of the planets of our Solar System. It is also a numerical integration of the Earth orientation and Moon rotation. Besides the classic planet equations of motion given in (Moyer, 2000), specific developments were done especially related to the Mars motion, the Earth rotation and the Moon libration. A special effort was done in the minimization of the roundoff errors during the integration processes. The integrator is an Adams-Cowell method with fixed step-size, and the programming is done in C language, thus allowing to use the extended precision (80 bits) on Intel Itanium II processors.

The development strategy was to built in a first stage a solution (called INPOP05) as close as possible to the DE405 JPL solution. INPOP05 was constructed as a test bed to demonstrate our capabilities in planetary solution computing and to understand as much as possible the rotation and orbital motion equations used in DE405. Some small differences still remain between the two solutions. Indeed, different choices were made in asteroid perturbation computations, in deformation of the Earth due to tide effects, and in the computations of the positions and velocities of the Sun versus the Solar System barycenter. Estimations of the differences are presented in subsection 2.3.6. An INPOP05 solution fitted to the same set of observations as DE405 will be presented in subsection 4.2.

In a second stage, a new dynamical model (INPOP06) was developed, following our best understanding of the dynamical equations. Section 2.4 introduces the INPOP06 dynamical model and section 5 presents the INPOP06 fit to observations.

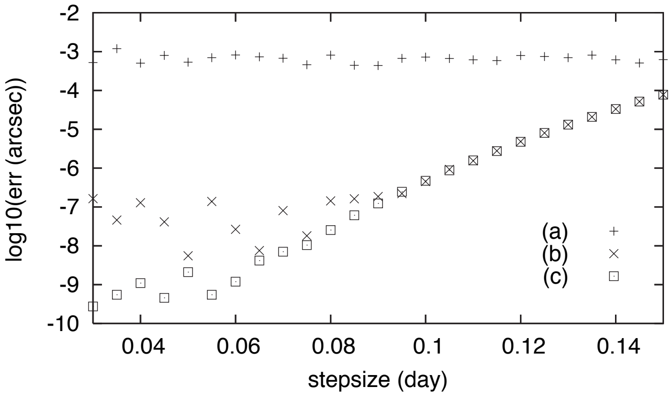

Fig. 1. Numerical error in the Moon longitude (in arcsecond) after 100 years for various settings :(a) double precision, (b) extended precision, (c) extended precision with a corrector step in simulated quadruple precision.

2.2. INPOP numerical integrator

The numerical integrations in INPOP are performed with a classical Adams PECE method of order 12 (e.g. Hairer *et al.* 1993) with the aim to reduce the roundoff error. For this, we have switched to extended precision on Intel architecture. The floating operations then use the 80 bits (with 64 bits mantissa) of the arithmetical unit instead of 64 bits (with 53 bits mantissa) for double precision. The improvement is very significant (Fig. 1) while the CPU cost is nearly the same (Markstein, 2000). In figure 1, the error in the computation of the Moon longitude after 100 years are computed for various step sizes by comparison with a very accurate solution obtained with the ODEX numerical integrator in quadruple precision and internal error set to 1E-28 (Hairer *et al.* 1993).

Integrating in quadruple precision would of course reduce the round off error in a very large amount, but the CPU time is about 15 time larger than for double precision arithmetic (or extended arithmetic) on our machine (Itanium II with Intel C++ compiler). Nevertheless, it was possible to obtain an additional order of magnitude improvement by using a single addition in simulated quadruple precision in the corrector step with a very small overhead.

Table 1. Estimated numerical error in longitude in INPOP06 (step size 0.055 day) for all planets i ($i = 3$ stands for the Earth-Moon Barycenter, and $i = 10$ for the Moon). The error ε_i is given in micro arc seconds (μas) or micrometers (μm) over 100 years and over 10000 years.

	100 yr		10000 yr	
i	$\varepsilon_i(\mu as)$	$\varepsilon_i(\mu m)$	$\varepsilon_i(\mu as)$	$\varepsilon_i(\mu m)$
1	3.3×10^{-4}	93.3	1.5×10^{-1}	41288
2	1.4×10^{-5}	7.5	9.3×10^{-3}	4901
3	1.9×10^{-5}	14.0	7.3×10^{-3}	5335
4	3.0×10^{-6}	3.4	4.2×10^{-4}	461
5	1.5×10^{-7}	0.6	9.0×10^{-6}	34
6	2.7×10^{-8}	0.2	5.3×10^{-6}	37
7	3.9×10^{-7}	5.5	1.7×10^{-6}	23
8	1.4×10^{-7}	3.1	1.3×10^{-6}	29
9	7.7×10^{-8}	2.2	1.3×10^{-6}	38
10	5.1×10^{-4}	1.0	1.3	2513

For the final integrations, the step size is chosen in order to minimize the roundoff error. For this, we take the largest step size for which the error is dominated by roundoff error and not by truncation error. This is monitored on the Moon longitude, for which the numerical error is the largest (Fig. 1). The final step size for INPOP06 has been chosen to 0.055 days, but during the fitting procedure, in order to improve CPU time, a 0.1 day step size was preferred.

Finally, with the chosen step size of 0.055 days, the numerical error for all planets has been estimated by an integration made over 10000 years one way and back. The results are displayed in Table 1. In this table, the error over 100 years is estimated by comparison to a high precision integration in quadruple precision with the ODEX integrator, while over 10000 years, the estimate of the error is the half of the difference obtained after integrating one way and back. Even over 10000 years, for most of the planets, the numerical error is so small that it has not reached an asymptotic behavior. For the Moon, the error in longitude behaves as $t^{1.46}$ (Fig. 2), following the optimal Brouwer's law in $t^{3/2}$ (Brouwer 1937, Quinn & Tremaine, 1990).

The analysis of the integration error over longer time intervals than 10000 years is beyond the scope of the present paper that is devoted to high accurate planetary ephemerides for astronomical observations and space mission design. One can thus consider that over the time span considered here (10000 years), with our numerical integrator design, the numerical error becomes completely negligeable (Table 1).

2.3. INPOP05 dynamical model: differences with DE405

Based on the equations developed by Moyer (2000) and used in the construction of the JPL DE numerical solutions, we have built the INPOP05 solution. Few elements differ between INPOP05 and DE405.

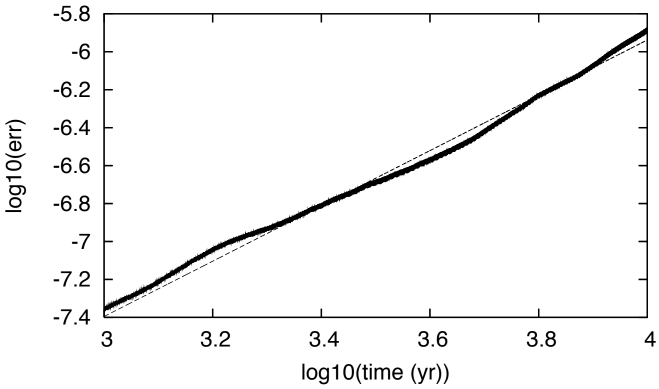

Fig. 2. Evolution of the roundoff error in the longitude of the Moon. The error (in arcsec) is estimated as the half of the difference after one way and back over 10000 years. The dashed line is obtained by least square adjustment, with slope 1.46.

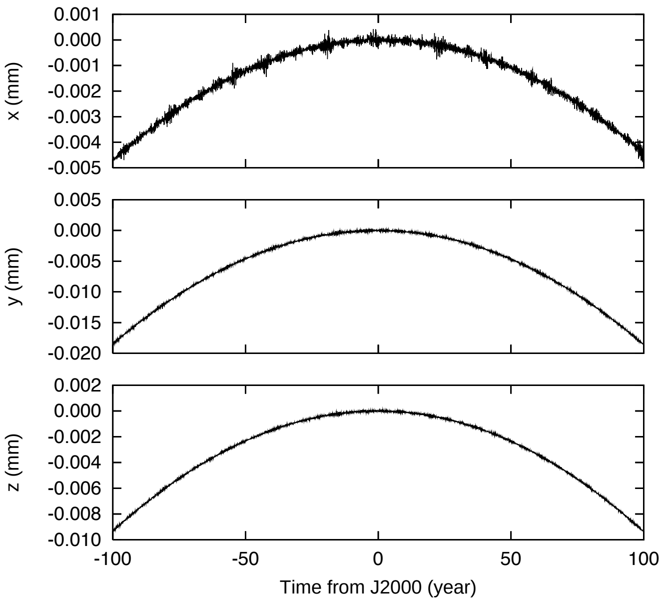

Fig. 3. These curves show the drift of SSB in INPOP. We consider here a simplified model, composed of the Sun, the planets from Mercury to Pluto and the Moon (no asteroids), all considered as point-mass bodies. At time origin of integration (J2000), the origin O of the reference frame is at the barycenter G of the system (Eqs 2, 4, 5). The curves show the drift of the barycenter G in the reference frame, that is $\boldsymbol{OG} = \left(\sum \mu_i^*\right)^{-1} \sum_i \mu_i^* \boldsymbol{r}_i$. Time interval is in years from J2000 and the coordinates of G are in mm.

2.3.1. Sun and Solar System barycenter

In JPL planetary solutions, the Sun is not integrated in the same way as the planets. Its position and velocity are determined from those of the planets and asteroids, assuming that the Solar System barycenter (SSB) remains at the origin of the inertial reference frame. If $\boldsymbol{r}_i$ is the barycentric position, $\boldsymbol{v}_i$ the barycentric velocity vector, and m_i the mass of body i, it is assumed that (see Le Poncin-Lafitte *et al.*, 2006)

$$\sum_i \mu_i^* \boldsymbol{r}_i = \boldsymbol{0} \tag{1}$$

with $\mu_i = Gm_i$ and up to order $1/c^2$,

$$\mu_i^* = \mu_i \left(1 + \frac{v_i^2}{2c^2} - \frac{1}{2c^2} \sum_{j \neq i} \frac{\mu_j}{r_{ij}}\right) . \tag{2}$$

By derivation of (1) we have

$$\sum_i \mu_i^* \dot{\boldsymbol{r}}_i + \dot{\mu_i^*} \boldsymbol{r}_i = \boldsymbol{0} \tag{3}$$

with, by derivation of (2) and up to order $1/c^2$,

$$\dot{\mu_i^*} = \frac{\mu_i}{2c^2} \left(\sum_{j \neq i} \mu_j \frac{(\boldsymbol{r}_j - \boldsymbol{r}_i) \cdot (\dot{\boldsymbol{r}}_j + \dot{\boldsymbol{r}}_i)}{r_{ij}^3}\right) \tag{4}$$

In INPOP, we have taken the term $\dot{\mu_i^*} \boldsymbol{r}_i$ into account. Moreover, the Sun is treated as the other planets without assuming a fixed SSB. Indeed, because of the approximations that are still made in the computation of μ_i^* and $\dot{\mu_i^*}$, there remains a small drift of the SSB in the fixed reference frame centered on the SSB at J2000. The determination of the SSB at the origin of time (J2000) is obtained by solving the equations

$$\begin{cases} \sum_i \mu_i^* \boldsymbol{r}_i = \boldsymbol{0} \\ \sum_i \mu_i^* \dot{\boldsymbol{r}}_i + \dot{\mu_i^*} \boldsymbol{r}_i = \boldsymbol{0} \end{cases} \tag{5}$$

where μ_i^* and $\dot{\mu_i^*}$ are given by equations (2) and (4). Because μ_i^* and μ_i^* are depending on planet velocities, an iterative process is needed. Contrarily to JPL method, these equations are solved only at the initial step of the planetary integration, at J2000. Once the frame is centered at the SSB defined by equations (5) at J2000, the equations of motion of planets and Sun are integrated in this fixed reference frame. Because of the approximations in $1/c^2$, the positions and velocities of the SSB deduced at t has still a very small displacement that can be neglected (Fig. 3).

One should note that if, as in the JPL model (Standish, 2004), the $\dot{\mu_i^*}$ term is neglected in the second equation of (5), a more important drift appears in the SSB motion (Fig. 4).

2.3.2. Asteroids

INPOP05 uses the same asteroid set as DE405 does. In DE405, the positions and velocities of asteroids are estimated with a Keplerian approximation. In INPOP05, all asteroid orbits are numerically integrated, taking into account the planetary perturbations on asteroids.

Once the asteroid positions and velocities are obtained, and in order to remain very close to the DE405 model, the INPOP05 computation of perturbations on planets does not differ from DE405: only asteroid perturbations upon Mars, the Earth and the Moon are taken into account for 297 of them (see section 2.4.1 for more details).

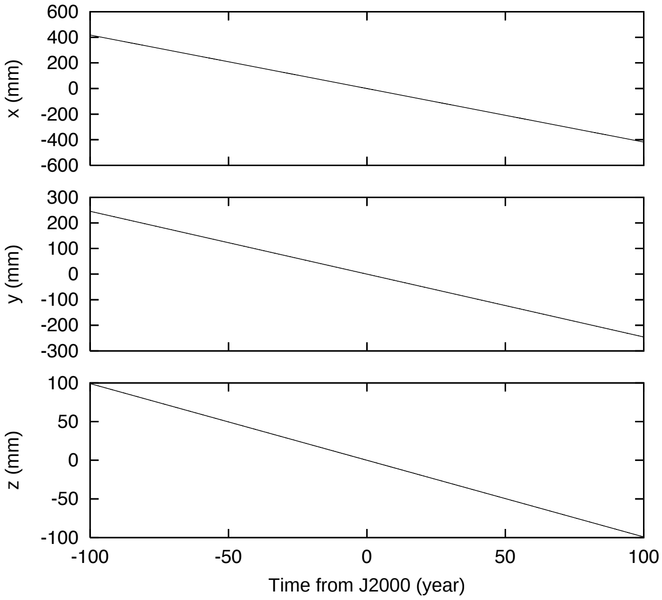

Fig. 4. Same kind of simulation as for figure 3 have been made, but in this case, $\dot{\mu_i^*}$ is neglected in (5) when computing the SSB at time origin of integration.

2.3.3. Earth tides

In DE102 and followers, only tides raised by the Moon on the Earth are considered (see equation II.C in Newhall et al. 1983).

In INPOP, Sun tides are added and the Earth shape varies with time: Earth coefficients of the potential are variable parameters. Expressions of their variations are given in (Lambeck, 1988).

$$\begin{cases} \Delta C_{20} = \dfrac{m_p}{M}\left(\dfrac{R}{r_p^*}\right)^3 \dfrac{k_{20}}{2} \dfrac{2r_z^{*2} - r_x^{*2} - r_y^{*2}}{r_p^{*2}} \\ \Delta C_{21} = \dfrac{m_p}{M}\left(\dfrac{R}{r_p^*}\right)^3 k_{21} \dfrac{r_x^* r_z^*}{r_p^{*2}} \\ \Delta C_{22} = \dfrac{m_p}{M}\left(\dfrac{R}{r_p^*}\right)^3 \dfrac{k_{22}}{4} \dfrac{r_x^{*2} - r_y^{*2}}{r_p^{*2}} \\ \Delta S_{21} = \dfrac{m_p}{M}\left(\dfrac{R}{r_p^*}\right)^3 k_{21} \dfrac{r_y^* r_z^*}{r_p^{*2}} \\ \Delta S_{22} = \dfrac{m_p}{M}\left(\dfrac{R}{r_p^*}\right)^3 \dfrac{k_{22}}{2} \dfrac{r_x^* r_y^*}{r_p^{*2}} \end{cases} \tag{6}$$

In these equations, m_p is the mass of the tide rising body (Sun or Moon), M and R are respectively the mass and the mean equatorial radius of the Earth, k_{2m} is the Love number associated to the harmonic $2m$. The vector $\boldsymbol{r_p}^*$ of the Earth-tide rising body, is estimated with a time delay τ_{2m}, depending on the order of the harmonic $2m$: $\boldsymbol{r_p}^* = \boldsymbol{r_p}\,(t - \tau_{2m})$. $\boldsymbol{r_p}^*$ is given in Earth's frame.

2.3.4. Earth orientation

When interactions with the figure of the Earth are computed, the knowledge of the Earth orientation is needed. It is the case for the computation of interactions between the non-spherical Earth and point-mass bodies, of the deformation of the Earth and of the torque exerted on the Moon due to the interaction between the non-spherical Earth and the non-spherical Moon. As in DE405, in INPOP05 the orientation of the Earth's axis is obtained with the precession model of (Williams 1994) and the nutation expression of (Wahr 1981), limited to the main 18.6 yr term.

2.3.5. Moon deformations

As for the Earth, in INPOP, the Moon is assumed to be a deformable body, shaped by its own rotation and the tides raised by the Earth. The Moon potential coefficients are time varying and the same coefficient developments as in section 2.3.3 are used. However, Love numbers and time delay are assumed to be independent of the order of the harmonic. Furthermore, as in DE405, variations of the Moon inertia tensor due to the Moon rotation is estimated following (Newhall et al. 1997). Variations of the coefficients of potential are then

$$\begin{cases} \Delta C_{20} = \dfrac{kR^3}{3GM}\dfrac{1}{2}\left(\omega^{*2} + 2n^2 - 3\omega_z^{*2}\right) \\ \Delta C_{21} = -\dfrac{kR^3}{3GM}\omega_x^*\omega_z^* \\ \Delta S_{21} = -\dfrac{kR^3}{3GM}\omega_y^*\omega_z^* \\ \Delta C_{22} = \dfrac{kR^3}{3GM}\left(\omega_y^{*2} - \omega_x^{*2}\right) \\ \Delta S_{22} = -\dfrac{kR^3}{3GM}\dfrac{1}{2}\omega_x^*\omega_y^* \end{cases} \quad (7)$$

In these expressions, k is the Love number (the same for all harmonics), R is the mean equatorial radius, G is the gravitational constant, M is the mass of the Moon, $\boldsymbol{\omega}^*$ is the instantanous vector of rotation (estimated with a time delay τ, that is $\boldsymbol{\omega}^*(t) = \boldsymbol{\omega}(t-\tau)$) and n is the mean motion of the Moon around the Earth.

2.3.6. Comparison to DE405

In order to analyze the differences between DE405 and the INPOP05 model, we have first integrated INPOP05 with the same initial conditions and parameters as for DE405. Using the initial conditions and constant values given in the DE405 header, we integrate INPOP05 over the whole time interval of DE405 (-400 yr to 200 yr with origin at J2000). Maximum differences obtained between DE405 and INPOP05 are shown in table 2. The agreement between the two ephemeris is very good, especially for the estimation of the Lunar geocentric positions. One should notice that these differences, except for Mars, are in general much smaller than the residual of the comparisons with the observations (see section 4.2). For Mars, the differences are larger than the other planets due to the computations of the asteroid orbits which are different between DE405 and INPOP05 or INPOP06. In table 2, the maximum differences between DE405 and INPOP05 for the three libration angles can be found for several intervals of time. In this case, again, the agreement between the two ephemeris is very satisfactory.

Table 2. Maximum difference between DE405 and INPOP05 (with the same initial conditions) in range (r), latitude (ϕ) and longitude (λ). If (x, y, z) are the heliocentric (geocentric for the Moon) coordinates of the planet in the equatorial reference frame of the ICRF, then $r = \sqrt{(x^2+y^2+z^2)}$, $\phi = \arcsin(z/r)$ and $\lambda = \arctan(y/x)$. EMB is the Earth-Moon Barycenter. For the librations of the Moon, ϕ, θ and ψ are the usual Euler's angles (see Newhall et al., 1983, section II.D). Comparisons are made over the whole time interval of DE405 (-400 yr to 200 yr with origin at J2000); Col.1: from -30 yr to +30 yr; Col.2: from -100 yr to +100 yr; Col.3: from -400 yr to 200 yr.

Heliocentric range r (m)			
Mercury	6.2	26	228
Venus	0.5	2.1	18
EMB	1.6	7.7	60
Mars	58	517	3365
Jupiter	31	108	467
Saturn	20	36	121
Uranus	38	45	69
Neptune	35	77	80
Pluto	31	119	283
Moon (geocentric)	0.009	0.034	0.540
Longitude λ (μas)			
Mercury	174	749	6637
Venus	78	534	6270
EMB	32	286	2494
Mars	354	6600	42070
Jupiter	57	276	1012
Saturn	16	51	201
Uranus	4	14	41
Neptune	0.7	14	39
Pluto	0.9	7	44
Moon (geocentric)	60	170	6173
Latitude ϕ (μas)			
Mercury	65	268	2373
Venus	30	207	2262
EMB	13	113	979
Mars	152	2602	16970
Jupiter	23	102	383
Saturn	5	17	67
Uranus	0.6	5	15
Neptune	0.2	5	14
Pluto	0.4	3	19
Moon (geocentric)	25	73	2478
Lunar librations (μas)			
ϕ	900	900	1000
θ	400	400	400
ψ	800	800	5800

2.4. A new dynamical model: INPOP06

Once we have verified, with INPOP05, that we are able to match very closely the JPL DE405 solution, we have started to construct the new model INPOP06, that will differ more significantly from the DE405 model. Indeed, we have searched for a dynamical model that follows our best understanding of the planetary and rotational dynamics of the Solar System, with the aim to reach the accuracy of the observations that will be available with the next space missions (Venus Express, GAIA, Bepi Colombo...). We have also searched for a solution that is as self consistent as possible, avoiding input of parts that are computed in a separate manner (as for the precession of the Earth for example).

We thus have different options for the Earth orientation and deformation, and we also use a more developed model for asteroid perturbations.

2.4.1. Asteroids

As INPOP05, INPOP06 sees asteroids as planet-likes. Their orbits are numerically integrated together with the planets.

The same 300 asteroids are used in INPOP06 and INPOP05, however the computation of their perturbations on planets differ. In INPOP05 and DE405, only the perturbations induced by Ceres, Pallas and Vesta are taken into account for all the planets. The other 297 perturbations are summed and used only for the Earth, the Moon and Mars orbit computations. In INPOP06, the perturbations of all the 300 asteroids upon all the planets are taken into account. As Fienga & Simon (2005) have shown, this induces significant drifts in the inner planet orbits. Fit to observations of the 5 largest asteroid masses (Ceres, Pallas, Vesta, Iris and Bamberga) and of the 3 taxonomic densities (C, S, and M) are made in INPOP06. The Krasinsky et al (2002) proposition of adding an asteroid ring potential in the inner planet orbit computations is also extended to the outer planets.

The asteroid ring is assumed to be cicular, with radius r_0 and mass M, and centered at the Solar System barycenter. The perturbed body with barycentric position vector $\boldsymbol{r}$ is supposed to be in the ring plane (the mutual inclination of the planets is neglected). Let $(\boldsymbol{u}, \boldsymbol{v})$ be a direct orthogonal basis in the ring plane, with $\boldsymbol{u} = \boldsymbol{r}/r$, and let $\boldsymbol{r'}(\theta) = r_0(\cos\theta \boldsymbol{u} + \sin\theta \boldsymbol{v})$ be the position vector of a point of the ring. The acceleration of the body due to the ring is:

$$\ddot{\boldsymbol{r}} = \frac{GM}{2\pi} \int_0^{2\pi} \frac{\boldsymbol{r'(\theta)} - \boldsymbol{r}}{\|\boldsymbol{r'(\theta)} - \boldsymbol{r}\|^3} \, d\theta \ . \tag{8}$$

Expressed in $(\boldsymbol{u}, \boldsymbol{v})$, one obtains:

$$\ddot{\boldsymbol{r}} = \frac{GM}{2\pi} \int_0^{2\pi} \frac{(r_0 \cos\theta - r)\boldsymbol{u} + r_0 \sin\theta \boldsymbol{v}}{\left(r^2 + r_0^2 - 2rr_0 \cos\theta\right)^{3/2}} \, d\theta \ . \tag{9}$$

For an inner body ($r < r_0$), (9) can be expanded in Fourier series using Laplace coefficients (see Laskar, 2005) and after averaging over θ, one finaly obtains:

$$\ddot{\boldsymbol{r}} = \frac{GM}{2rr_0^2} \left(b_{3/2}^{(1)}(r/r_0) - \frac{r}{r_0} b_{3/2}^{(0)}(r/r_0) \right) \boldsymbol{r} \ . \tag{10}$$

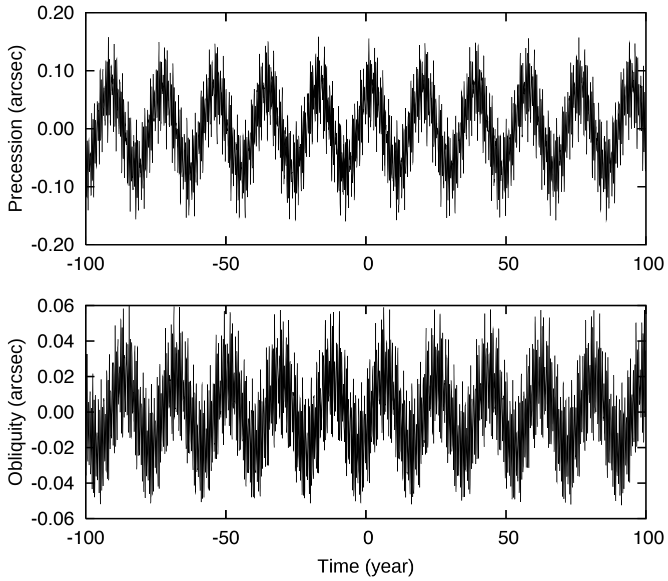

Fig. 5. Discrepancies in Earth's orientation between INPOP06 and the CIP-P03 in precession and obliquity (units are in arcsec). Comparisons are made over the interval -100 yr to +100 yr with origin at J2000.

This expression is equivalent to the one exposed in (Krasinsky et al. 2002) in term of hypergeometric functions. For an outer body ($r > r_0$), the same developpements lead to the expression of the acceleration of an outer body due to the asteroid ring:

$$\ddot{\boldsymbol{r}} = \frac{GM}{2r^3} \left(\frac{r_0}{r} b_{3/2}^{(1)}(r_0/r) - b_{3/2}^{(0)}(r_0/r) \right) \boldsymbol{r} \ . \tag{11}$$

In INPOP06, the mass of a circular asteroid ring with 2.8 AU radius centered at the Solar System barycenter is fitted to observations.

2.4.2. Earth deformations

The Earth deformations are modeled as described in section 2.3.3. Secular variation of the Earth J_2, due to the postglacial rebound of the mantle, is also taken into account in the computation of the acceleration and torques applied on the Earth with the constant rate ($\dot{J}_2 = -3 \times 10^{-9}/cy$). This value was determined by satellite laser ranging (Yoder et al., 1983) and is used by (Williams, 1994) and by (Capitaine et al., 2005) in the precession model P03 that has been recently adopted by the IAU (IAU 2006 resolution 1)[1].

[1] In the P03 model, $\dot{J}_2 = -3.001 \times 10^{-9}/cy$, but the $0.001 \times 10^{-9}/cy$ coefficient is meaningless owing the very coarse relative precision of the determination of this value. Indeed, it should be noted that a significant change in $\dot{J}_2$ has been recently observed (Cox et al., 2002).

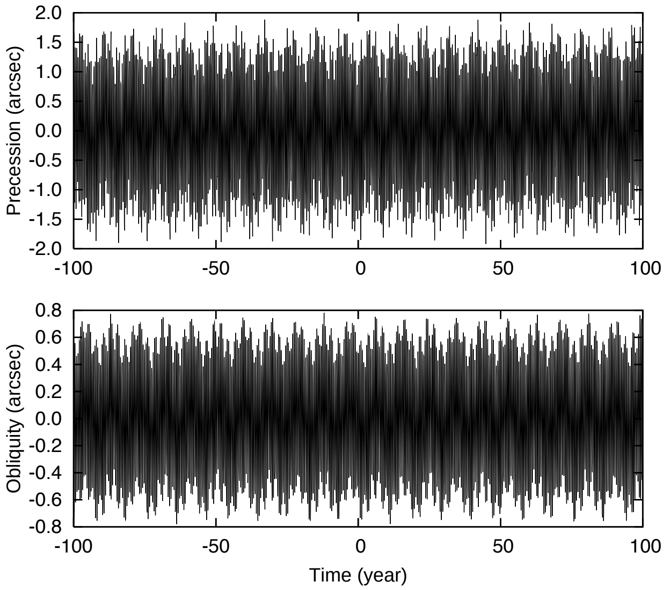

Fig. 6. Discrepancies in Earth's orientation between the Earth's pole used to compute DE405 (precession of Williams (1994) and the single 18.6 yr nutation term from Wahr (1981)) and the CIP-P03 in precession and obliquity (units are in arcsec). Comparisons are made over the interval -100 yr to +100 yr with origin at J2000.

2.4.3. Earth orientation

In INPOP06, the Earth orientation is integrated at the same time as all other bodies and Moon libration. With INPOP05 and DE405, the Earth orientation was estimated with (Williams, 1994) and (Wahr, 1981) precession and nutation models. These two models are based on some planetary ephemeris, and are expressed in term of periodic and polynomial terms that are valid only over a few thousand years. Then, inconsistencies between the Earth orbital and rotational motion can appear. In order to allow longer time integrations, and ensure the self-consistency of the solutions, we have chosen to integrate the rotational motion of the Earth together with its orbital motion.

The numerical integration of the full rotational motion of the Earth would require a very small step size, based on the rotational frequency of the Earth (ω). Following (Boué & Laskar, 2006), we have chosen here to average over the rotational motion of the Earth. Indeed, if A, B, C are the principal momentum of inertia of the Earth, $\boldsymbol{K}$ is the unit vector in the direction of the largest momentum of inertia C, and $\boldsymbol{w} = \boldsymbol{G}/G$ the unit vector in the direction of the rotational angular momentum of the Earth, the averaged value $< \boldsymbol{K} >$ of $\boldsymbol{K}$ is extremely close to $\boldsymbol{w}$. Indeed (Boué & Laskar, 2006),

$$< \boldsymbol{K} >= \boldsymbol{w} + O(J^2) \ , \tag{12}$$

where J is the angle between $\boldsymbol{K}$ and $\boldsymbol{w}$. From the solution for a rigid Earth SMART97 (Bretagnon et al., 1998), it can be deduced that for the Earth, $|J| < 1.22 \times 10^{-7}$ rad and $J^2 = O(10^{-14})$. The orientation vector $\boldsymbol{K}$ vector can thus be replaced by the $\boldsymbol{w} = \boldsymbol{G}/\|\boldsymbol{G}\|$ angular momentum vector. The evolution of the angular momentum, up to term in $O(J^2)$ is given by (Boué & Laskar, 2006)

$$\dot{\boldsymbol{G}} = 3\frac{2C-(A+B)}{2\|\boldsymbol{G}\|^2}\sum_i \frac{\mu_i}{r_i^5}\left(\boldsymbol{r}_i \cdot \boldsymbol{G}\right)\boldsymbol{r}_i \wedge \boldsymbol{G} \ , \tag{13}$$

where $\boldsymbol{r}_i$ are the position vector of the perturbing bodies ($i = 1, ...9$ is the index for the Moon, Sun and all planets except the Earth from Mercury to Neptune). All quantities are expressed in the fixed frame of integration. The initial conditions for the unit vector $\boldsymbol{w} = \boldsymbol{G}/\|\boldsymbol{G}\|$ and form parameter C/MR^2 (where C is the largest moment of inertia, M the mass, and R the mean equatorial radius of the Earth) are fitted on the CIP-P03 pole in the ICRF reference frame (Capitaine et al., 2005) over 200 years around J2000. The fitted value for C/MR^2 is 0.330821725.

Figure 5 shows the differences between the integration of Earth's orientation with INPOP06 and the CIP-P03. The differences, smaller than 0.2 arcseconds in angle of precession and 0.07 arcseconds in obliquity, are due to the "free core nutations", not taken into account in our integration. It should be noted that we compare here the mean angular momentum vector $\boldsymbol{w}$ integrated in INPOP06 with the CIP-03 that is an approximation of the attitude vector $\boldsymbol{K}$. The differences of $\boldsymbol{w}$ with the true angular momentum of the Earth would be even much smaller as the angular momentum is not affected (at first order) by the liquid core contribution.

It should also be pointed out that the approximation of the attitude vector of the Earth $\boldsymbol{K}$ that we obtain by computing $\boldsymbol{w}$ is much more accurate than the approximation of $\boldsymbol{K}$ that is presently used in the JPL ephemeris models (Fig. 6), both models being adequate for the computation of orbital ephemeris.

Finally, over time intervals longer than 1000 years, the differences between the computed Earth orientation in INPOP06 and the CIP-P03 start to diverge significantly (Fig. 7). This results from the presence of polynomial approximations in the precession angles of the CIP-P03. Beyond about 2000 years, the errors in the secular terms of the CIP-P03 precession formulas will exceed the short period discrepancies between INPOP06 and CIP-P03 resulting from the consideration of the liquid core in CIP-P03 (Fig. 5).

3. Planetary ephemeris overview

Recent evolutions of JPL and IMCCE planetary ephemeris have an important impact on the quality of these solutions. Since 1998, the JPL DE405 solution is the worldwide reference for planetary ephemeris. It is used at JPL and ESA to prepare space missions. As it was demonstrated by Standish & Fienga (2002), the uncertainty on the main belt asteroid masses induces inaccuracies on the Mars heliocentric and geocentric orbits. In the same time, several Mars missions took place since 1998 (Pathfinder, Mars Global Surveyor, Mars Odyssey) providing new informations that can be used to better constrain asteroid

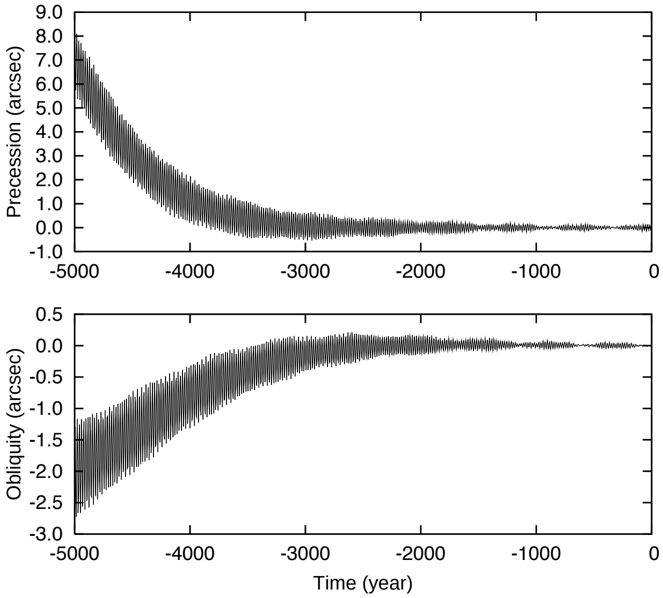

Fig. 7. Discrepancies in Earth's orientation between INPOP06 and the CIP-P03 in precession and obliquity (units are in arcsec). Comparisons are made over -5000 yr with origin at J2000.

perturbations. Several new solutions including these data were then built by JPL (DE410, DE414) and by IMCCE (INPOP06). The main differences between these solutions are the asteroid perturbations modeling and the Mars observations used in the fit. In DE411, perturbations induced by a ring were applied on Mars and Earth orbits. The observational interval for DE411 fit is from 1899 to January 2004, including MGS data. In DE414, in addition of ring perturbations, more than 64 asteroid masses were estimated with the DE414 fit including MGS and Mars Odyssey data till April 2005. As far as we know at the time we write this paper, DE414 is the most advanced JPL solution for Mars.

4. INPOP observational processing and adjustment

The complete data processing dedicated to planetary ephemeris fit was well presented in Standish (1990). However, we explicit here some differences in the INPOP processing of data.

Three main types of observations are used for planetary ephemeris fits: direct radar observations of the planet surface (Venus, Mercury and Mars), spacecraft tracking data (radar ranging, Doppler and VLBI), and optical observations (transit, photographic plates and CCD observations for outer planets).

4.1. Observational processing

4.1.1. Mercury and Venus

For Mercury and Venus, a large part of the observations are direct radar observations. The signal is emitted by an antenna and reflected directly by the planet surface. This kind of observations are not very accurate because they are strongly correlated with our knowledge of the planet topography. Usually, the uncertainties of these observations are a few kilometers. To correct the data from surface topography, we use different models. More specifically, we use for Venus the Rapaport & Plaut (1994) model based on the Magellan observations, and for Mercury, the Anderson et al. (1996) model based on Doppler observations of the Mercury surface done from 1967 to 1990. The INPOP fit is based on JPL observations realized from 1971 to 1997 for Mercury and from 1964 to 1990 for Venus.

For direct radar observations, the Anderson et al (2005) solar corona modeling is applied. This model includes the latest estimation of solar electronic density from the Cassini mission. The relativistic correction is given by Moyer (2000). When a tropospheric correction is needed, we applied the simplified model given by Standish (1990).

VLBI observations of the Venus orbiter, named Magellan, were obtained in the early nineties (Folkner 1992, 1993, 1994a, 1994b). They are VLBI measurements of the spacecraft with respect to background sources from a radio source catalogue. Thanks to these observations, it is possible to tie the INPOP inner planet system to the ICRF radio frame.

4.1.2. Mars

For Mars, different types of observations are involved. In the INPOP fit, we choose to take into account only the space tracking data arguing than the few kilometers accuracy of the direct radar observations of the Mars surface can be put apart compared to the few meters accuracy of the modern space observations. One will see from the comparisons between DE405 and INPOP05 that this hypothesis seems to be justified (see section 4.2). Viking, Pathfinder, MGS and Mars Odyssey observations were used in the fit. These missions have furnished orbiter ranging, lander ranging (Viking and Pathfinder missions) and differenced range, and orbiter VLBI observations (MGS mission).

For direct radar observations and spacecraft radar ranging, the procedure is very similar. In principle, relativistic, tropospheric and plasma (solar corona) corrections are applied in the same manner. However, for spacecraft tracking data, some corrections (usually the tropospheric correction, and sometimes the plasma correction) were applied by the navigation teams.

The orbiter ranging data are distances furnished by the JPL navigation teams, which means that they are free from spacecraft orbits. They are distances from the Mars center of mass to the antenna at the Earth surface. The reduction to the geocenter is done in the IERS frame, using IAU 2000 recommendations for precession, nutation and Earth orientation parameters.

The processing of the Viking and Pathfinder lander ranging data are more complex because the data are distances from the Mars surface where the lander is situated to the Earth surface where the antenna is located. Mars rotation modelings must then be introduced. Some publications such as EPM (Pitjeva 2005) give fitted rotation model parameters and lander coordinates obtained during the planetary ephemeris fit. For INPOP, we decided to use the values of the IAU Mars rotation parameters (Seidelmann et al., 2002) and the (Lyttleton et al., 1979) Mars nutation model. The lander coordinates are the one computed by JPL (Standish, 1998).

The processing of the lander Doppler observations corresponds to differenced radar range observations (Yeomans et al 1992). Differences are computed between two round-trip time intervals observed at few seconds. Estimations of rate variations of the Mars lander to Earth antenna distances are then obtained. Because such observations could be seen as radial velocity estimations, they are usually called Doppler observations. The same modelings as the one described previously for Mercury, Venus and Mars ranging are used for Doppler including the Mars rotation correction induced by lander situation. Description of the Viking and Pathfinder differenced range is done in Folkner et al (1997).

MGS VLBI data were obtained during the orbit of the spacecraft to Mars. Here again, these data are differenced VLBI data. Spacecraft angular positions versus the observed radio sources are estimated. Since the spacecraft orbit is well known, the navigation teams deduced angular positions of planets versus the reference radio sources. These data, with the Venus Magellan and the Jupiter Galileo observations, increase the connections between the dynamical system based on INPOP planetary ephemeris and the ICRF.

4.1.3. Outer planets

To tie the INPOP outer planets plane to the same ICRF reference plane as inner planets, 44 VLBI differenced observations obtained during the Galileo missions are used in the Jupiter orbit fit. These data were also provided by JPL navigation teams. A complete description can be found in Folkner(1998).

For Jupiter and Saturn, besides old direct optical observations of the planets, observations of satellites are taken into account in the fit. The major source of systematic errors in the outer planet astrometry is the phase effect. Due to the lightening gradient and the scattering law, the determination of the center of mass relative to the photocenter, is very difficult. Several methods were tested to correct these effects (Fienga and Delouis 2001, Fienga 1999) but better accuracies are obtained from satellite observations (Fienga 1998). As their surface are telluric and their apparent diameters are much smaller, modelings of the phase effect are easier and most of the time the satellite phase defect is neglected. Moreover, the dynamical theories of satellites were developed with the use of various observations and are more precise than the Jupiter or Saturn ephemeris itself (Vienne and Duriez 1995, Arlot 1982). The combination of accurate relative positions of satellites and observed right ascension and declination of good quality allows us to obtain accurate equatorial coordinates of the planets. The problem of the phase effect of the planets is then removed.

For Uranus, Neptune and Pluto, we used direct observations of the planets. Considering the accuracy reached by the transit, photographic and CCD observations, phase effects can be neglected. For Pluto VLT observations, this assumption is not true and phase effect correction must be applied.

Common treatments related to reference frames are applied to all optical observations. As INPOP plane of reference must be linked with ICRF, each outer planet optical observations are expressed in ICRF following IAU 2000 recommendations. Depending on the publication frames of the data, different algorithms are applied. For old observations, corrections from FK3 to FK4 and FK4 to FK5 frames are applied (Yallop 1989, Frike 1971). FK5 zonal corrections are also taken into account (Schwan, 1988) and rotations from the FK5 to the ICRF (Mignard and Froeschlé, 1998) are applied. Such transformations guarantee, at the level of accuracy of the optical data (about 100 mas), the link between the INPOP outer planet frame and ICRF. Galileo VLBI observations orbiting Jupiter enforce this link at the VLBI accuracy which means a factor 100 improvement compared to the optical observations tie.

4.2. INPOP05 fit to observations and comparison to DE405

In order to validate our fitting process, we have first fitted INPOP05 with the same samples of observations than those used to obtain DE405. Postfit residuals are shown in table 3.

For Mercury and Venus, no topography model is fitted but the model described in section 5 is used. Due to these differences in topography, INPOP05 residuals seem slightly better than DE405 ones. Again with Mars, no fit of the Viking lander coordinates is done and no direct radar observations of Mars are included in the fit. Despite this, differences between INPOP05 and DE405 residuals are very small. For outer planets, the fit includes direct observations of the planet photocenter and positions deduced from satellite observations. As in DE405, besides the planet initial conditions, 3 asteroid masses, 3 asteroid taxonomic classes are fitted to observations.

Besides these small differences, very similar results are obtained for INPOP05, meaning that the fitting process is valid. Such a check was necessary before developing some new independent fitted solutions.

5. INPOP06

After building a twin ephemeris of DE405 (see section 2.3), dynamical modeling improvements are done and a fit is

Table 3. INPOP05 (Column 6) and DE405 (Column 5) residuals for each type of observations. Column 3 gives the time interval of observations and Column 4 the number N of observations used in the fit and in the residual computations. For optical observations, the residuals are given respectively in right ascension and declination (α; δ). The given uncertainties are given at 1-sigma.

Planet	Type of Data	Time Interval	N	DE405	INPOP05
Mercury	Radar [m]	1971-1998	415	-515.0 $\pm$ 982	- 520.0 $\pm$ 951
Venus	Radar [m]	1964-1990	510	- 3613.0 $\pm$ 4688	- 3384.0 $\pm$ 4749
	Spacecraft VLBI [mas]	1990-1994	18	1.6 $\pm$ 3	1.6 $\pm$ 3
Mars	Vkg lander radar [m]	1976-1983	1253	0.44 $\pm$ 13	0.37 $\pm$ 12.5
Jupiter	CCD or transit (α,δ) [mas]	1914-1994	2872	(- 32 $\pm$ 480 ; - 31 $\pm$ 472)	(- 32 $\pm$ 480 ; - 31 $\pm$ 472)
Saturn	CCD or transit (α,δ) [mas]	1914-1994	2339	(- 52 $\pm$ 503 ; - 20 $\pm$ 454)	(- 52 $\pm$ 504; - 19 $\pm$ 454)
Uranus	CCD or transit (α,δ) [mas]	1914-1994	2909	(50 $\pm$ 400 ; 8 $\pm$ 403)	(50 $\pm$ 400 ; 9 $\pm$ 401)
Neptune	CCD or transit (α,δ) [mas]	1914-1994	2830	(78 $\pm$ 437 ; -51 $\pm$ 400)	(78 $\pm$ 436 ; -52 $\pm$ 396)
Pluto	CCD or transit (α,δ) [mas]	1989-1993	208	(- 54 $\pm$ 266 ; - 14 $\pm$ 258)	(- 62 $\pm$ 270 ; - 18 $\pm$ 255)

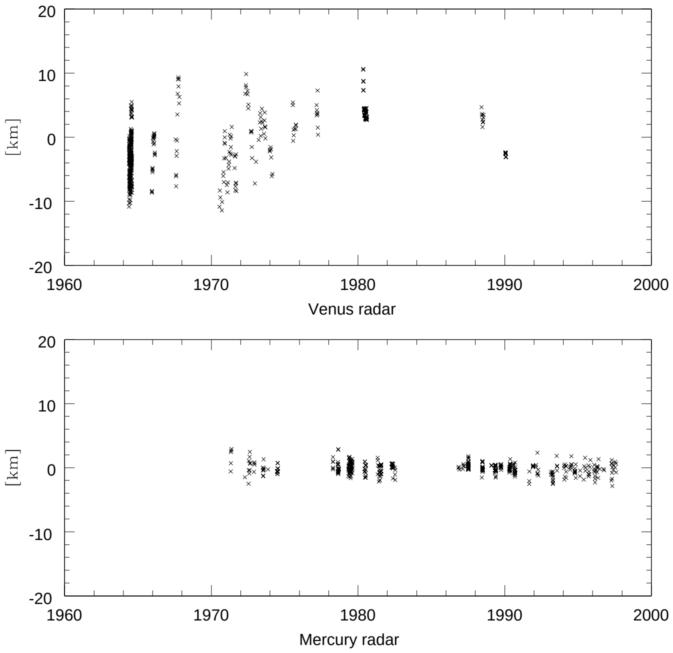

Fig. 8. Mercury and Venus direct radar observation comparison to INPOP06. y-axis is given in kilometers and x-axis is dates.

possible with all available observations. A new independent planetary ephemeris, called INPOP06, is then built. We describe in the following sections the fit to the observations and the comparisons to DE414. Tests to independent new Mars Express observations are also presented.

5.1. New features in observational fit

The fit of INPOP06 was done using observations until June 2005 while the JPL DE414 numerical solution (Konopliv et al. 2006) is fitted to the most recent MGS and Mars Odyssey observations until April 2005. Our INPOP fitting interval is thus two months longer than the DE414 one, but this should not be the main source of differences between the two solutions.

For Jupiter and Saturn, only angular positions deduced from satellite observations are taken into account in the INPOP06 fit. We have made this choice because they are more accurate than the direct observations of the planet photocenter and because the time interval covered by the satellite observations is longer than the orbital period of the planet. A complete observational cover of the planet orbit is then guaranteed. Due to the limited interval of time covered by the Uranian and Neptunian satellites observations, it was not possible to make the same choice for Uranus and Neptune.

In addition to the planet initial conditions, we also fit 5 asteroid masses, 3 taxonomic classes, the ring mass (its distance to the Sun is fixed to 2.8 UA) and the Sun oblateness (J2). Fitted physical parameters are presented in table 7. Different values extracted from other planetary ephemeris are also presented in this table. One can find the values obtained with DE414, DE405 and EPM04. The EPM04 solution (Pitjeva 2005) is a numerical ephemeris of the planets and Moon very similar to DE414, fitted on the Mars space observations and including supplementary Russian data.

5.2. Comparison INPOP06 fitted - DE405

Maximum differences between INPOP06 fitted to observations and DE405 are presented in table 4 over several intervals of time.

For the planets, the differences are important due to the changes in the dynamical model (asteroid perturbations over all the planets, use of an asteroid ring) and to the fit made with new observations. Especially for Mars, the differences in heliocentric longitudes induce a difference of about 200 meters in geocentric distances. Such effect is mainly due to the more complex modelisation of the asteroid perturbations and to the observational fit realised on MGS/MO data. These data are five time more accurate

Table 4. Maximum difference between DE405 and INPOP06 in range (r), latitude (ϕ) and longitude (λ). If (x, y, z) are the heliocentric (geocentric for the Moon) coordinates of the planet in the equatorial reference frame of the ICRF, then $r = \sqrt{(x^2 + y^2 + z^2)}$, $\phi = \arcsin(z/r)$ and $\lambda = \arctan(y/x)$. EMB is the Earth-Moon Barycenter. For the librations of the Moon, ϕ, θ and ψ are the usual Euler's angles (see Newhall et al., section II.D). Comparisons are made over the whole time interval of DE405 (-400 yr to 200 yr with origin at J2000); Col.1: from -30 yr to +30 yr; Col.2: from -100 yr to +100 yr; Col.3: from -400 yr to 200 yr.

Heliocentric range r (m)			
Mercury	690	1 100	1 700
Venus	3 000	3 000	3 000
EMB	31	51	163
Mars	87	690	3 000
Jupiter	77 000	110 000	170 000
Saturn	320 000	330 000	370 000
Uranus	760 000	770 000	840 000
Neptune	980 000	3000 000	3000 000
Pluto	8300 000	27000 000	49000 000
Moon (geocentric)	0.009	0.09	2
Longitude λ (μas)			
Mercury	14 000	24 000	56 000
Venus	24 000	40 000	96 000
EMB	1 300	1 600	4 000
Mars	1 300	8 500	41 000
Jupiter	120 000	300 000	1200 000
Saturn	170 000	250 000	320 000
Uranus	170 000	200 000	540 000
Neptune	120 000	390 000	850 000
Pluto	270 000	1400 000	8400 000
Moon (geocentric)	1 400	2 700	31 000
Latitude ϕ (μas)			
Mercury	14 000	16 000	29 000
Venus	14 000	20 000	37 000
EMB	2 000	2 000	2 200
Mars	1 900	4 400	17 000
Jupiter	47 000	130 000	430 000
Saturn	68 000	99 000	140 000
Uranus	47 000	75 000	210 000
Neptune	78 000	110 000	390 000
Pluto	26 000	550 000	3700 000
Moon (geocentric)	2 000	2 100	13 000
Lunar librations (μas)			
ϕ	8 500	8 500	8 700
θ	4 100	4 200	4 300
ψ	7 400	7 400	29 000

than the Viking observations, which were the only spacecraft data used in Mars DE405 adjustement and thanks to the MGS/MO sample, the Mars space missions observational time interval is now extended over 30 years.

In INPOP06, the Moon orbit and rotation modelisations are the same as in INPOP05. However, as modifications were done in the INPOP06 planet dynamical model and a new observational fit was made, the Moon solution changed. To stay close to the DE/LE405 solution of lunar motion (which is fitted on LLR observations), a fit of the Moon geocentric initial conditions and time delays (τ_{21} and τ_{22} for the Earth, τ for the Moon) was done on the DE/LE405 Earth-Moon distance. In table 4, one may see that the differences between DE/LE405 and INPOP06 Moon solutions stay reasonable in geocentric longitude, latitude and distance as well as in libration angles. The values of the time delays deduced from the fit of the INPOP06 Moon and the ones used for DE/LE405 can be found in table 5.

Table 5. Time delay values used in DE405 (and INPOP05) (col. 2), and in INPOP06 (col. 3), used to compute the tidal effects (see sections 2.3.3 and 2.3.5). τ_{E21} and τ_{E22} are respectively Earth's time delays for harmonics (2,1) and (2,2), and τ_M is the one for the Moon. They are expressed in days and rounded to 10^{-10}.

Time delays	DE405	INPOP06
τ_{E21}	0.0129089594	0.0129645035
τ_{E22}	0.0069417856	0.0069368125
τ_M	0.1667165558	0.1667744540

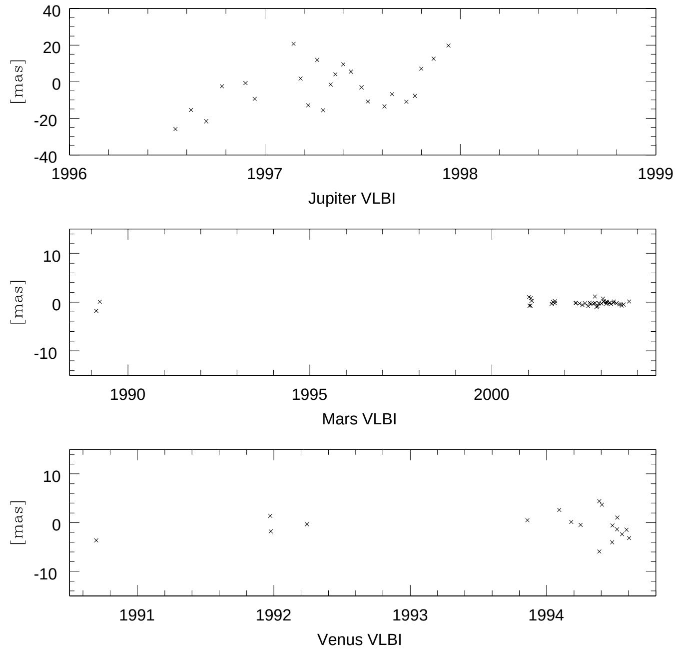

Fig. 9. Venus, Mars and Jupiter VLBI observation comparison to INPOP06. y-axis is given in mas and x-axis is dates

5.3. Comparison INPOP06 fitted - DE414

In table 6, one may find the INPOP06 and DE414 postfit residuals. Figures 8, 9 and 10 illustrated the residuals obtained with INPOP06 after fit.

For Mercury and Venus, one may notice smaller residuals for INPOP06 than DE414. The residual dispersion between INPOP06 residuals and DE414 ones decreased from about 9% for Mercury and 3 % for Venus. The bias is also reduced by a factor more than 5 for Mercury and 3 for Venus between the 2 solutions. This could be explained by

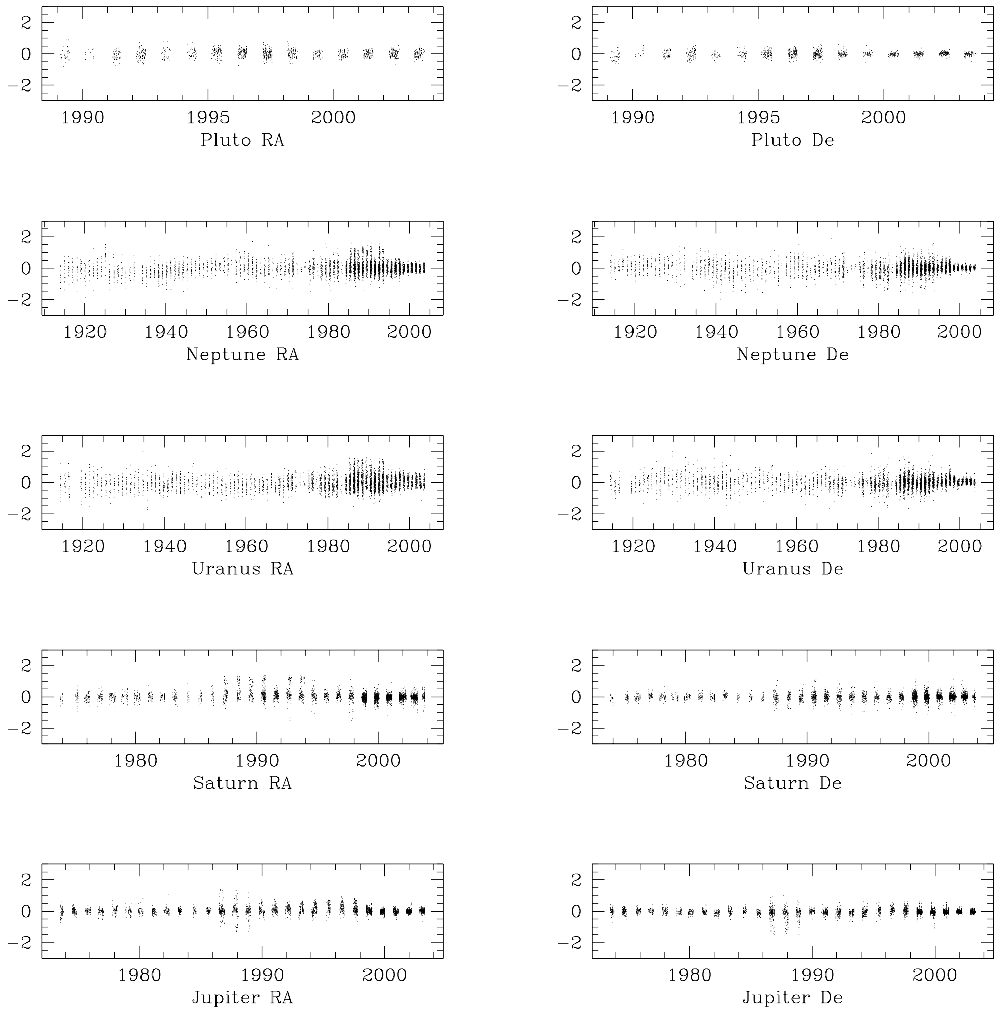

Fig. 10. Outer planet optical observations comparison to INPOP06. y-axis is given in arcseconds and x-axis is dates

the asteroid perturbations included in the INPOP06 modeling. Fienga and Simon (2005) have shown the important impact of these perturbations on the Mercury heliocentric and geocentric distances. As far as it was communicated to us, no asteroid perturbations were included in the DE414 solution. One may also notice than no topography model is fitted in INPOP fit contrary to the DE414 fit.

For Mars, the DE414 fit induces more than 64 asteroid mass fits besides the inclusion of the asteroid ring. Compared to INPOP06 which has a very similar modeling (including asteroid ring perturbations) but has only a fit of 5 asteroid masses, the DE414 fit seems to be more complete and gives better results. In Figure 12 and 13, one may see the smoother behavior of the DE414 MGS residuals compared to the INPOP residuals. In table 6, one may see that over very short time period (comparison to MGS/MO data) but also over long time period (comparison to Viking data), DE414 solution seems to be better fitted to observations than INPOP06 does. However, considering the INPOP06 and DE414 differences and weighting schemes, INPOP06 can be seen as a very competitive independent solution. In the following section, one may see that comparisons to observations not used in INPOP nor DE414 fits will give an interesting estimation of the two solutions extrapolation capabilities.

VLBI residuals are very similar for INPOP06 and DE414. ICRF ties of the 2 solutions seem to be done with the same accuracy.

For outer planets, better dispersion residuals are obtained with INPOP06. However, these improvement are not homogeneous and are more sensitive in right ascension than in declination. Based on the estimation of mean elements, one may establish the frame tie between INPOP06 and ICRF.

5.4. Fit of physical parameters

On table 7, the fitted values of physical parameters computed by INPOP06 are gathered. Values extracted from other planetary solutions are also shown. One can see

Table 6. INPOP06 (Column 6) and DE414 (Column 5) residuals for each type of observations. Column 3 gives the observational time interval and Column 4 the number of observations N used in the fit and in the residual computations. For optical observations, the residuals are given respectively in right ascension and declination (α;δ). The given uncertainties are given at 1-sigma.

Planet	Type of Data	Time Interval	N	DE414	INPOP06
Mercury	Radar[m]	1971-1998	444	-596.0 ± 956	-107.8 ± 871
Venus	Radar[m]	1964-1990	511	- 3578.0 ± 4671	- 1126.0 ± 4527
	Spacecraft VLBI[mas]	1990-1994	18	1.7 ± 2.5	0.6 ± 3
Mars	Vkg lander radar [m]	1976-1983	1256	-5.7 ± 18	0.2 ± 20
	MGS/MO radar [m]	1999-2005.45	10474	7.4 ± 4.1	2.5 ± 7.5
	MGS/MO radar DE414 data sets [m]	1999-2005.3	10287	1.55 ± 3.5	2.52 ± 7.6
	Vkg lander Doppler [mm/s]	1976-1979	1501	-0.26± 4.5	-0.25 ± 4.4
	Pathfinder lander Doppler [mm/s]	1997	1519	-0.34 ± 0.97	-0.34 ± 0.97
	Spacecraft VLBI [mas]	1989-2003	44	0.04 ± 0.5	0.1 ± 0.5
Jupiter	Spacecraft VLBI [mas]	1996-1998	24	-1 ± 12	3 ± 12
	CCD or transit (α,δ) [mas]	1973-2004	3189	(47 ± 222 ; 36 ± 198)	(24 ± 214 ; - 26 ± 190)
Saturn	CCD or transit (α,δ) [mas]	1973-2004	3863	(29 ± 280 ;- 1 ± 196)	(- 28 ± 270 ; - 2 ± 196)
Uranus	CCD or transit (α,δ) [mas]	1914-2004	3848	(11 ± 440 ; 13 ± 370)	(0.5 ± 351 ; 4 ± 361)
Neptune	CCD or transit (α,δ) [mas]	1914-2004	3898	(12 ± 404 ; 11 ± 438)	(-0.4 ± 360 ; 0.5 ± 350)
Pluto	CCD or transit (α,δ) [mas]	1989-2004	1024	(13 ± 264 ; -0.8 ± 252)	(0.9 ± 250 ; - 47 ± 190)

the great consistency of the values between different solutions. The larger value of the solar J_2 estimated by DE414 could be explained by the lack of asteroid perturbations in the Mercury and Venus orbits in the DE solutions. Such perturbations are taken into account in the EPM04 and INPOP solutions. One can notice that our fitted value of J_2 ($1.95 \pm 0.55 \times 10^{-7}$) is still in good agreement with the helioseismic determination ($J_2 = 2.18 \pm 0.06 \times 10^{-7}$) (Pijpers 1998). The INPOP determination of the Sun oblateness J_2 was done with the fixed standard values for the PPN parameters ($\beta = \gamma = 1$), but we have also performed some tests on the β, γ determinations during the INPOP06 fit to observations. With the fixed value of the Sun oblateness $J_2 = 1.95 \times 10^{-7}$, the best residuals are obtained with $|\beta - 1| < 10^{-5}$. On the other hand, if J_2 and β are considered as free parameters, then the best combination for residual minimization is $J_2 = 2.5.10^{-7} \pm 0.55$ and $|\beta - 1| < 10^{-4}$. Determinations of γ were done after fixing the J_2 and the β parameters. As one can see in table 8, the results are consistent with the values obtained with the planetary solutions EPM04 and EPM06 (Pitjeva 2005, 2006). One could note that the determination of β with INPOP06 are significantly more precise than the values published by Will (2006), obtained during the reduction process of other kind of data (spacecrafts time delays and VLBI observations).

5.5. Comparison with independent observations: MEX tracking data

5.5.1. MEX mission

Mars Express (MEX) is the first European mission to Mars. Launched on 2 June 2003 for a 5 years mission,

Table 8. RG tests based on INPOP06 fit to observations. In the first column, one may find the publications from where the values are extracted and the methods used to estimate the Sun J2 and the PPN parameters β and γ. In columns 2, 3 and 4, computed values of these parameters can be found.The given uncertainties are given at 1-sigma.

	Sun J2 10^{-7}	$\lvert\beta - 1\rvert$ 10^{-5}	$\lvert\gamma - 1\rvert$ 10^{-5}
This paper			
INPOP06	1.95	< 1	< 2
INPOP06	2.50 ± 0.55	< 10	< 2
(Pitjeva, 2005)			
EMP04	1.9 ± 0.3	(0 ± 10)	(-10 ± 10)
(Pitjeva, 2006)			
EMP06	2 ± 0.5	< 20	< 20
(Will, 2006)			
Cassini tracking			(2.1 ± 2.3)
VLBI			(0 ± 40)
Heliosismology	2.2 ± 0.1	(0 ± 300)	

the spacecraft is now orbiting Mars in a polar orbit of 87 degrees inclination, pericenter altitude of 250 km, and orbital period 7.5 h. The scientific payload of Mars Express orbiter comprises seven instruments, providing stereoscopic imaging, spectral coverage from ultraviolet to the infrared, and radar sounding of Mars (Chicarro, 2003). MEX navigation is done by ESOC based on JPL DSN and ESA tracking observations. MEX tracking observations are round trip time interval between the space-

Table 7. Physical parameters fitted in INPOP06. Other values deduced from planetary solutions are presented for comparisons.The given uncertainties are given at 1-sigma.

	Unit	DE405	EPM 04	DE414	INPOP06
Mass of Ceres	$10^{-10}M_\odot$	4.64	4.753 ± 0.007	4.699	4.746 ± 0.006
Mass of Vesta	$10^{-10}M_\odot$	1.34	1.344 ± 0.001	1.358	1.338 ± 0.002
Mass of Pallas	$10^{-10}M_\odot$	1.05	1.027 ± 0.003	1.026	0.995 ± 0.003
Mass of Iris	$10^{-10}M_\odot$		0.063 ± 0.001	0.060	0.089 ± 0.002
Mass of Bamberga	$10^{-10}M_\odot$		0.055 ± 0.001	0.047	0.060 ± 0.002
Mass of Ring	$10^{-10}M_\odot$		3.35 ± 0.35	0.329	0.34 ± 0.15
Distance of Ring	UA		3.13 ± 0.05	2.8	2.8
Density of the C class		1.8	1.4	1.6 ± 0.22	1.93 ± 0.12
Density of the S class		2.4	3.5	2.07	2.13 ± 0.11
Density of the M class		5.0	4.5	4.3 ± 0.43	4.47 ± 0.012
Sun J2	10^{-7}	2	1.9 ± 0.3	2.3 ± 2.5	1.95 ± 0.55

craft orbiting Mars and the antenna on the Earth surface. Thanks to the Earth-Mars distance, the angular effect due to the orbital motion of the spacecraft around Mars center of mass is neglected. ESA (Morlay 2006) provides us observational sets cleaned from MEX orbit corrections (AMDs, Mars potential and solar panel accelerations) on about one year time interval containing more than 19000 observations with about 10 % obtained with the new European tracking network in Australia (New Nortia). As MEX observations were never used in planetary ephemeris fits, they are very useful to test the extrapolation capabilities of planetary ephemeris. Furthermore, they are the first data sets which were not proceeded by the JPL navigation teams. Consequently, they are free from possible dependencies between JPL navigation procedures and JPL planetary ephemeris fitted on observations produced by the same navigation algorithms.

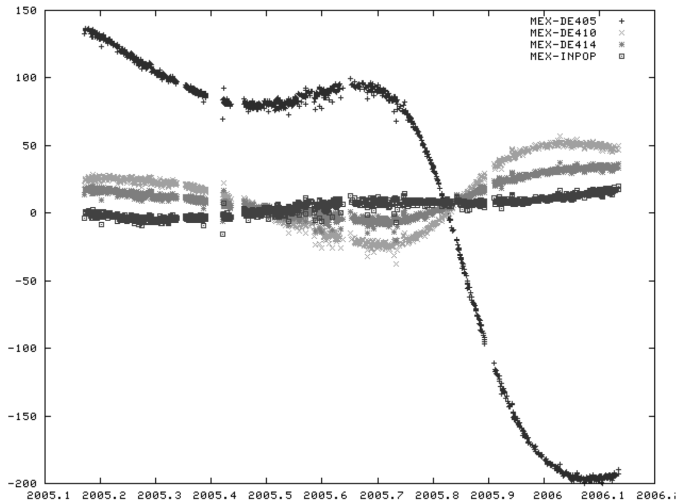

Fig. 11. MEX residuals in meters to DE405 (black), DE410 (light gray), DE414 (gray) and INPOP06 (deep gray)

5.5.2. Complete data set

The complete MEX observation interval provided by ESA is from 2005.18 to 2006.2.

On Figure 11, the differences in meters between observed MEX geocentric distances and DE405, DE410 and INPOP06 Mars-Earth distances are plotted. One can see the important improvement obtained from DE405, DE410, DE414 and INPOP06 solutions. The remaining quadratic trend in DE410, DE414 and INPOP06 residuals could be expected to disappear after a fit of the planetary solution to MEX data. This trend would correspond to perturbations induced by asteroids with badly known masses.

With the DE414 and INPOP06 solutions, better estimations of the Mars geocentric distances are expected since their fits were proceeded on observations done partly simultaneously with the MEX data. Fig 12 and Fig 13 present the residuals of MGS and MEX data to respectively DE414 and INPOP06. With DE414, one can see a good behavior of the solution with the MGS data but a very rapid degradation with the MEX observations. With INPOP06, the residual statistics with the fitted MGS data are less impressive than the DE414 one, but its extrapolation capability is slightly better. Table 9 gathers the statistics related to theses comparisons.

5.5.3. Overlap data set

DE414 and INPOP06 fit data sets have common time intervals with the MEX observations: for DE414, [2005.18: 2005.3] and [2005.18: 2005.45] for INPOP06. On these overlap intervals, it is interesting to study the statistics of the residuals obtained by comparisons between the MGS and MEX observations and the two planetary solutions. Because, the solutions are fitted on these time intervals, the MEX residuals would be cleaned from effects due to unfitted perturbations and then from effects due to Mars

Table 9. MEX and MGS residuals in meters to DE414 and INPOP06. Statistics are given in mean and 1-sigma dispersion.

Observations	Time interval	DE414	INPOP06	DE410	DE405
MGS residuals [m]	1999.1-2005.43	7.6 ±4.1	2.5 ± 7.6	2.3 ± 4.5	
MEX residuals [m]	2005.18-2006.2	11.2 ± 12.1	8.3 ± 6.7	14.3 ± 25.2	27.8 ± 112.3

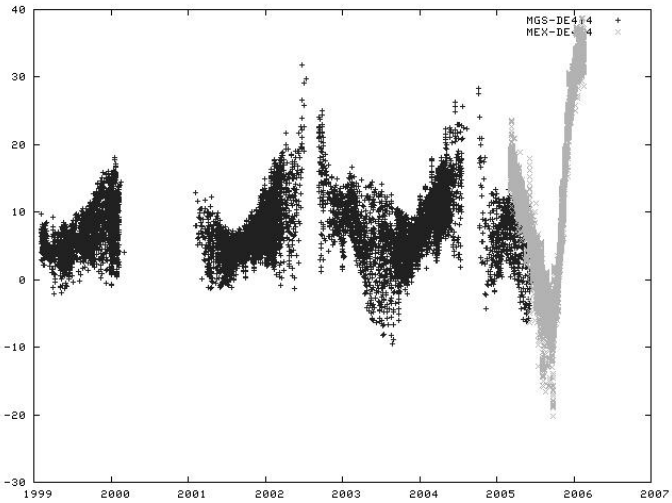

Fig. 12. MGS (black dot) and MEX (gray dot) residuals in meters to DE414

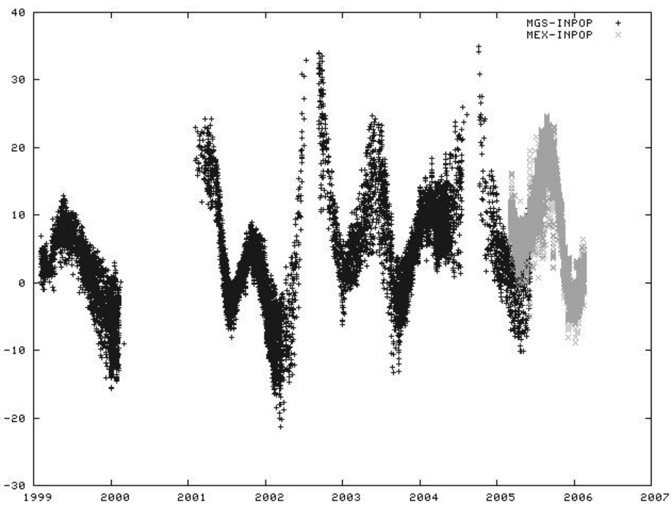

Fig. 13. MGS (black dot) and MEX (gray dot) residuals in meters to INPOP06

and Earth motion imperfect modelisation. Only observational effects would remain. With such comparisons, one can estimate the intrinsic accuracy of the MEX tracking observations. Fig. 14 and Fig. 15 present such residuals. Different behaviors can be seen for DE414 and INPOP06, but what appears commonly for DE414 and INPOP06 residuals is the better dispersion of the MEX data compared to the MGS observations. Residual statistics can be

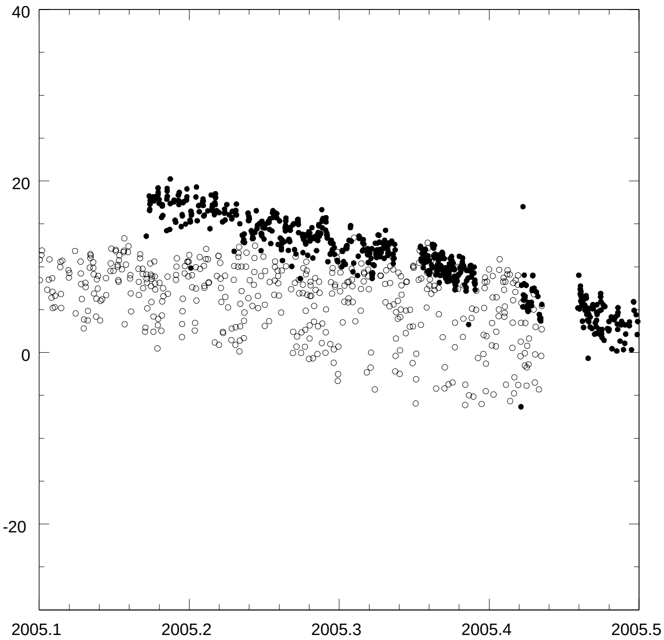

Fig. 14. MGS (open circle) and MEX (black dot) residuals in meters to DE414 on the overlap interval.

found in Table 10. One can see that the 1-sigma dispersion of the MEX data is about 2 meters compared to the 4 meters dispersion of the MGS residuals. Moreover, the bias of the MEX observations seems to be reasonable and consistent with the value expected by ESOC navigation team (about 10 meters).

6. Future developments and conclusions

In the previous section, we have presented our past work on the construction of a new independent numerical solution for the planet and Sun motions as well as Earth and Moon rotations. We have introduced the dynamical models used for the description of the planetary motion and rotations. We have shown how we analyzed planetary observations and how we proceed for the fit of the INPOP solutions to observations. Prefit and Postfit comparisons between the numerically integrated orbits and the observed positions are presented as well as tests of extrapolations using new MEX observations. These tests and comparisons show the good quality of our last INPOP06 solution especially when comparisons are done versus the last DE414 JPL ephemeris. One may notice that such good

Table 10. MEX and MGS residuals in meters to DE414 and INPOP06 on the overlap interval. Statistics are given in mean and 1-sigma dispersion.

Planetary Ephemeris	Time interval	MGS residuals in meters	MEX residuals in meters
DE414	2005.18-2005.3	6.5 ±3.6	15.2 ± 2.0
	2005.18-2005.43	5.6 ±4.4	12.6 ± 3.4
INPOP06	2005.18-2005.43	0.6 ± 4.5	7.3 ± 1.8

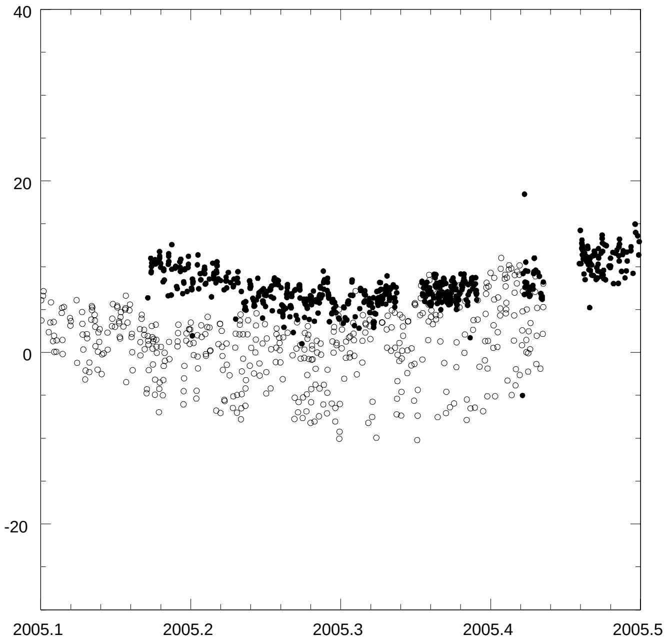

Fig. 15. MGS (open circle) and MEX (black dot) residuals in meters to INPOP06 on the overlap interval.

results were obtained in minimizing the number of fitted parameters. Only values of direct physical parameters not related to observational methods are determined from the INPOP06 fit. A public release of INPOP06 is available on the website **http://www.inpop.eu** with a tchebychev polynomial representation compatible with the JPL programs using JPL tchebychev files. An INPOP06 realization of the TCB time scale will be published.

Several new aspects and improvements will be investigated for the next INPOP version.

The Moon orbital solution and libration should be fitted directly to Lunar Laser Ranging (LLR) observations. LLR data will be used to estimate new initial conditions and libration paramaters as well as tests for new inner Moon models. Furthermore, a new LLR station based on adaptative optics (APOLLO) has begun to obtain very accurate observations (Murphy et al., 2002). Such new observations are very promising for a better understanding of the lunar dynamics and inner physics. In the same way as a inner Moon model has to be introduced, the INPOP Earth orientation could be improved by the introduction of a liquid core. With this addition, an improvement of about a factor ten could be expected in the comparisons between INPOP Earth orientation and P03.

Analysis of new observations based on the European tracking of the MEX and Venus Express (VEX) missions will bring new informations related to the very accurate modeling of the Mars and Venus orbits. New tests on the asteroid selection of perturbing objects are also to be done. The classification of the asteroids in three taxonomic classes can be improved. A new organization of asteroid families according to their dynamical properties has to be tested. Especially, the VEX observations will be very important because since the Magellan mission in the nineties, no accurate data were obtained for the Venus orbit.

Finally, in order to densify the sets of data used for the reference frame tie, a new link to the ICRF can be attempted in using millisecond pulsar timings. Progresses in pulsar timing observations and reduction procedures (Hobbs et al., 2006) make thus these data interesting in the Earth orbit fit and the construction of a pulsar catalogue linked to ICRF by pulsar VLBI observations can allow indirect connection between ICRF and the INPOP dynamical frame.

Acknowledgements. We thank M. Standish for multiple dicussions along this work. N. Capitaine and all the participants of the working group on planetary ephemeris (GTEP) held at Paris Observatory are thanked for their input to this work. The authors especially thank the ESA/ESOC navigation team of the interplanetary missions MEX and VEX for providing us the tracking data of the spacecrafts and for their help and explanations. This work was supported by CNES under contract 05/CNES//00-DCT 094, by the CS of Paris Observatory, and by PNP-CNRS.

References

Anderson, J.D., Laing, P.A., Lau, E.L., Liu, A.S., Nieto, M. M., Turyshev, S.G 2005, arXiv, 0104064,

Anderson, J.D., Jurgens, R.F., Lau, E.L., Slade, M.A., III, Schubert, G. 1996, Icarus, 124, 690

Arlot, J.-E. 1982, A&A, 107, 305

Boué, G., laskar, J. 2006, Icarus, in press , ,

Bretagnon, P., Francou, G., Rocher, P., Simon, J.-L. 1998, A&A, 329, 329
Brouwer, D. 1937, AJ, 46, 149
Capitaine, N., Wallace, P. T., Chapront, J. 2005, A&A, 432, 355
Chicarro, A.F. and The MEX Science Team 2003, Sixth International Conference on Mars, 3049,
Cohen, C. J., Hubbard, E. C., Oesterwinter, C. 1967, AJ, 72, 973
Cox, C.M., Chao, B. 2002, Science, 297, 831
Fienga, A., Simon, J.-L. 2005, A&A, 429, 361
Fienga, A., Delouis, J.M. 2001, A&A, 368, 1115
Fienga, A. 1999, BAAS, 31, 1589
Fienga, A. 1998., A&A, 335, 1111
Folkner, W.M. 1992, JPL IOM, 335.1, 92
Folkner, W.M. 1993, JPL IOM, 335.1, 93
Folkner, W.M. 1994a, JPL IOM, 335.1, 94
Folkner, W.M. 1994b, JPL IOM, 335.1, 94
Folkner, W.M., Kahn, R.D., Preston, R.A., Yoder, C.F., Standish, E.M., Williams, J.G., Edwards, C.D., Hellings, R.W., Eubanks, T.M., Bills, B. G. 1997, J. Geophys. Res., 102, 4057
Fricke, W. 1971, A&A, 13, 298
Hairer, E., Nordsett, S. , Wanner, G.: 1993, Solving Ordinary Differential Equations, Vols. I, Second Edition, *Springer–Verlag*
Hobbs, G.B., Edwards, R.T., Manchester, R.N. 2006, MNRAS, 369, 655
Konopliv, A.S., Yoder, C.F., Standish, E.M., Yuan, D.-N., Sjogren, W.L. 2006, Icarus, 182, 23
Krasinsky, G.A., Pitjeva, E.V., Vasilyev, M.V., Yagudina, E.I 2002, Icarus, 158, 98
Lambeck, K. 1988, Clarendon Press, ,
Laskar, J 2005, Celest. Mech., 91, 351
Laskar, J., Correia, A.C.M., Gastineau, M., Joutel, F., Levrard, B., Robutel, P. 2004a, Icarus, 170, 343
Laskar, J., Robutel, P., Joutel, F., Gastineau, M., Correia, A.C.M., Levrard, B. 2004b, A&A, 428, 261
Laskar, J. 1990, Icarus, 88, 266
Laskar, J. 1989, Nature, 338, 237
Laskar, J. 2005, Celestial Mechanics and Dynamical Astronomy, 91, 351
Le Poncin-Lafitte, C., Manche, H., Fienga, A., Laskar, J. 2006, private communication, ,
Lyttleton, R.A., Cain, D.L., Liu, A.S. 1979, NASA STI/Recon Technical Report, 79, 33140
Markstein, P.: 2000, IA-64 and Elementary Functions, *Prentice Hall, New Jersey*
Mignard, F., Froeschlé, M. 1998., Highlights of Astronomy, 11, 313
Moyer, T. 2000, ed. Joseph H. Yuen, John Wiley & Sons,
Morlay, T. 2006, priv. comm., ,
Murphy, T.W., Aldelberg, E.G., Strasburg, J.D., Stubbs, C.W. 2002, in Thirteenth International Workshop on Laser Ranging, Washington D.C., on October 07 through 11, 2002
Newhall, X. X., Standish, E. M., Williams, J. G. 1983, A&A, 125, 150
Newhall, X. X., Williams, J. G. 1997, Celestial Mechanics and Dynamical Astronomy, 66, 21
Pijpers, F.P. 1998, MNRAS, 297, L76
Pitjeva, E.V. 2006., Nomenclature, Precession and New Models in Fundamental Astronomy, 26th meeting of the IAU, Joint Discussion 16
Pitjeva, E.V. 2005, Solar System Research, 39, 176
Quinn, T., Tremaine, S. 1990, AJ, 99, 1016
Rappaport, N., Plaut, J.J. 1994, Icarus, 112, 27
Seidelmann, P.K., et al. 2002, Celes. Mech. and Dyn., 82, 83
Schwan, H. 1988, A&A, 198, 363
Standish, E.M. 2005, private comm., ,
Standish, E.M. 2004, A&A, 417, 1165
Standish, E.M., Fienga, A. 2002, A&A, 384, 322
Standish, E.M. 1995, JPL IOM, 314.10, 127
Standish, E.M. 1998, JPL IOM, 312.F, 98
Standish, E.M. 1990, A&A, 233, 272
Vienne, A., Duriez, L. 1995, A&A, 297, 588
Wahr, J.M. 1981, Geophys. J. Roy. Astron. Soc., 64, 705
Will, C. M. 2006, Living Rev. Relativity, 9, 3
Williams, J.G. 1994, AJ, 108, 711
Yallop, B.D., Hohenkerk, C.Y., Smith, C.A., Kaplan, G.H., Hughes, J.A., Seidelmann, P.K. 1989., AJ, 97, 274
Yeomans, D.K., Chodas, P.W., Keesey, M.S., Ostro, S.J., Chandler, J.F., Shapiro, I.I. 1992, AJ, 103, 303
Yoder, C.F., Dickey, J.O., Schultz, B.E., EANES, R.J., Tapley, B.D. 1983, Nature, 303, 391